IEEE Access
Multidisciplinary | Rapid Review | Open Access Journal

Received September 20, 2020, accepted October 5, 2020, date of publication October 12, 2020, date of current version October 22, 2020.

Digital Object Identifier 10.1109/ACCESS.2020.3030307

Quantitative Imaging Detection of Additive Manufactured Parts Using Laser Ultrasonic Testing

YI JIANG[1], HAITAO WANG[1], SHUAI CHEN[1], QING ZHANG[1], PAN HU[1], XIN LI[1], KAI ZHENG[2], AND HAILONG WANG[3]

[1]College of Automation Engineering, Nanjing University of Aeronautics and Astronautics, Nanjing 210016, China
[2]Jiangsu Special Inspection Institute, Nanjing 210036, China
[3]Shandong Great Wall Computer System Company Ltd., Nanjing 210000, China

Corresponding authors: Haitao Wang (htwang2002@126.com) and Yi Jiang (jiangyi12@nuaa.edu.cn)

This work was supported in part by the National Natural Science Foundation of China under Grant 61903193, in part by the Jiangsu Innovation Program for Graduate Education under Grant KYCX18_0267, in part by the Special Public Welfare Industry Research of the State Administration of Quality Supervision, Inspection and Quarantine under Grant 2015424068, and in part by the Key Laboratory of Non-Destructive Testing and Monitoring Technology for High-Speed Transport Facilities of the Ministry of Industry and Information Technology.

ABSTRACT Selective laser melting (SLM) is an important method of additive manufacturing, however it has some disadvantages such as poor surface qualities of the formed parts and the appearances of small surface defects. In this article, 360L stainless steel with artificial defects in different lengths are processed by SLM processing. A full noncontact laser ultrasonic-based B-scan detection system is built to detect the surface defects. The interaction between the scattered surface wave and the surface defect is verified through 3-dimension (3D) finite element simulation. In order to improve the signal-to-noise ratio (SNR) of laser ultrasonic signal in AM 316L part, Variational Mode Decomposition (VMD) algorithm based particle swarm optimization (PSO) is applied to denoise signals. Meanwhile, wavelet transform (WT) algorithm is used to compare SNR with VMD algorithm. Then, the time and amplitude parameters of different positions are extracted to realize B-scan imaging, and the lengths of defects are further accurately quantified through the time-amplitude-position imaging images. Otherwise, we find that the size of laser spot affects the precise quantification of defects. The smaller the spot is, the more precise the quantitative effect is. The results show that this method can quantitatively detect surface defects of AM 316L parts.

INDEX TERMS Additive manufactured, laser ultrasonic testing, quantitative imaging, surface wave, VMD.

I. INTRODUCTION

Overview of the National Industrial Development, the demands for high strength steel and other metal structures are increasing, and the performance requirements are also becoming higher. Additive manufacturing (AM) technology arises at this environment [1], [2]. SLM is a method of AM [3], [4], and the mechanical properties of the parts produced can be comparable to the traditional casting parts [5].However, small defects will destroy the mechanical properties of the metal materials [6], [7], resulting in the process being unable to continue and even the workpiece being scrapped [8]–[10].Therefore, it is particularly important to carry out quantitative and effective testing for AM products with non-destructive testing. At present, Nilsson [11] used ultrasonic eddy current and X-ray methods to detect the artificial defects of TC4 titanium alloy additive test blocks. du Plessis *et al.* [12], Dikshit *et al.* [13], and *et al.* [14] applied X-ray microcomputed tomography in AM. Ziółkowski *et al.* [15] and Zanini *et al.* [16] used CT detections technology to detect the porosity, pore size and orientation of 316L stainless steel parts and Ti6Al4V sample made by laser selection melting. Kobayashi *et al.* [17] used eddy current testing method to detect the defects of internal circular holes in additive manufacturing with stepped and sloping surfaces. However, X-ray detection technology has potential radioactive hazards [18]. Eddy current testing is greatly influenced by the distance of lift-off [19]. Traditional ultrasonic testing (NDT) is a contact testing, which c is limited by the surface shape of the tested object.

The associate editor coordinating the review of this manuscript and approving it for publication was Vincent Chen.

However, laser ultrasound [20], [21] (LU) can realize completely non-contact detection through combining the laser excitation and the interferometer acceptance. In addition, the interaction between the laser ultrasound induced surface wave and surface defects has also been extensively studied in many different applications [22]–[27]. The National Research Council of Canada [28] adopted laser ultrasound combined with synthetic aperture focusing testing (SAFT) to detect the defects such as shallow surface pores, unfused and poor bonding in 718 alloy and TC4 titanium alloy. Cerniglia *et al.* [29] detected the sandwich cracks of the AM parts by B-scan, which verified the feasibility of using laser ultrasound for imaging detection of the AM parts. In addition, when the sizes of the crack are much smaller than the wave length of the surface wave, the variations of the echo signals of simple A-sweep surface wave are very weak, and it is difficult to detect the microdefects by this method. The scanning laser ultrasonic method can detect such small defects. Therefore, B-scan detection is applied in this article to detect small defects of different lengths [30].

Secondly, due to the influence of processing technology and material roughness of AM products, the signal received by a laser interferometer contains more noise interference, thus affecting the accuracy of quantitative detections. Therefore, noise reduction method is necessary. Common signal decomposition algorithms include Wigner-Ville distribution, Fri1, and wavelet transform [31]–[33]. However, there is cross interference with the Wigner-Ville distribution. The WT requires the signal in the window to be steady, while the laser ultrasonic signal is nonlinear and non-stationary. VMD can break the above algorithm limitations. This algorithm can adaptively separate complex signals and is very useful for the extraction of nonlinear and non-stationary characteristics of signals. This algorithm is also widely used in different field [34], [35]. Jiang *et al.* [36] accurately extracted the weak damage characteristic of the rotation fault by VMD algorithm. Yan and Jia [37] realized the identification of multi-fault rolling bearings through VMD feature extraction. Sun *et al.* [38] also used VMD algorithm to extract signal features and realize the classification and identification of sample unbalanced rolling bearings. However, few researches combine VMD algorithm with laser ultrasonic additive fabrication detection to realize high-precision nondestructive detection. Therefore, the VMD algorithm based on PSO was used for the first time in this article to decompose the laser ultrasonic signal and realize the high-precision quantitative detection of small defects in additive fabrication.

The contributions of this study are listed as follows.

1) This study firstly presents a full noncontact laser ultrasonic-based B-scan detection system to detect the AM surface defects.
2) The interaction between the scattered surface wave and the surface defect is verified through 3-dimension (3D) finite element simulation.
3) In order to improve the signal-to-noise ratio (SNR) of laser ultrasonic signal in AM 316L part, VMD algorithm based particle swarm optimization (PSO) was applied to process signals.
4) The time and amplitude parameters of different positions were extracted to realize B-scan imaging, the effects of the size of laser spot on precise quantification of defects are analyzed and considered to be the cause of the errors.

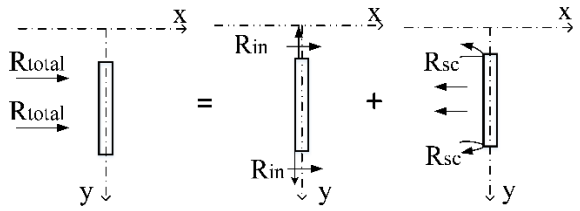

FIGURE 1. Scattering phenomenon of laser ultrasonic surface wave.

To sum up, the work of this article is mainly composed of the following parts. The part II mainly focuses on the diffraction principle of laser ultrasonic surface wave and the establishment of three-dimensional simulation. The interaction between surface wave and defects of different lengths is analyzed. The VMD algorithm based on PSO is described in part III. The preparation method of the specimen and the construction of the experiment are introduced in part IV. Experimental signal processing and imaging quantitative analysis are studied in IV part. The V part is the summary and discussion.

II. PRINCIPLE AND SIMULATION

A. PRINCIPLE OF LASER ULTRASONIC SCATTERING WAVE DETECTION

Under the thermal elastic effect of laser, the surface of the material has transient thermal expansion. The mode ultrasound is then produced. The surface wave energy ratio is the highest, mainly distributed in the material surface 2λ depth range. The surface wave has high sensitivity to the detection of surface small defects. Surface waves travel through the medium and interact with defects. According to Huygens principle, ultrasonic waves scatter and generate reflected and transmitted waves. As shown in the Fig.1. The sound field of the interaction between surface waves and defects can be expressed as:

$$R_{total}(x) = R_{in}(x) + R_{sc}(x), \tag{1}$$

where, $R_{total}(x)$ is the total sound field, $R_{in}(x)$ is the incident sound field, and $R_{sc}(x)$ is the scattered sound field. The scattered sound field consists of transmitted and reflected waves. When the ultrasonic wave length is larger than the defect length, most of the energy will bypass the defect (transmission). When the wavelength of ultrasonic wave is close to the defect length, part of the energy is transmitted and part is reflected. When the ultrasonic wave wavelength is smaller than the defect length, most of the energy is reflected and the later the arrival time is. Therefore, the defects can be judged according to the transmitted wave energy. Combined with the time delay of surface waves at different receiving positions, the defect length is further analyzed precisely and quantitatively.

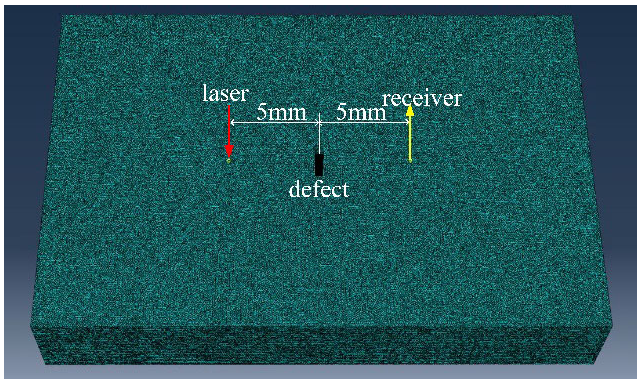

FIGURE 2. Laser ultrasonic finite element Simulation model (after meshing).

B. ESTABLISHMENT OF 3D SIMULATION MODEL

In order to analyze the interaction between ultrasonic surface waves and defects in different lengths, 3D finite element simulation is established in this article. The distribution of laser energy in time and space is approximately Gaussian distribution function. The distribution of laser energy in time and space can be expressed as $g(t)$ and $f(x, y)$ respectively:

$$g(t) = \frac{8t^3}{t_0^4} \exp\left(-\frac{2t^2}{t_0^2}\right), \tag{2}$$

$$f(x, y) = \frac{2}{R_G\sqrt{2\pi}} exp\left[-\frac{(x - x_G)^2 + (y - y_G)^2}{R_G^2}\right], \tag{3}$$

where, t_0 is the rising time of the laser, (x_G, y_G) is the coordinates of the laser center, and R_G is the radius of the laser point source. The heat flow energy generated by laser irradiation on the material surface can be described as:

$$Q = E_0 A f(x, y) g(t), \tag{4}$$

where, E_0 is the laser intensity at the incident center, A is the absorptivity absorbed on the material surface, and Q is the total energy absorbed on the material surface. In the time domain simulation, the stability of the numerical system and the spatial sampling of the wave mode are affected by two key factors, namely the time step size Δt and the spatial grid size Δx. If the time step is too long, the model will lose its stability. If the time step is too small, it will consume a lot of calculation time. Therefore, their selection follows the following principles:

$$\Delta t < \frac{1}{20 f_{max}}, \tag{5}$$

$$\Delta x < \frac{\lambda_{min}}{20}, \tag{6}$$

The 3D model is shown in Fig. 2. The length, width and height of the sample are 40mm × 20mm × 5mm respectively. The surface defect is represented by a rectangular groove perpendicular to the surface of the material. The width and depth of the defect are 0.5mm × 1mm, and the length of the defect is 0.8mm, 2mm and 6mm respectively. In order to avoid the influence of boundary reflection wave and reduce the calculation time of the model, absorption boundary is added around the model. The initial ambient temperature is set at room temperature of 300K and the mesh size is 0.1mm. The incident laser energy is 1mJ (thermoelastic state), the rise time of laser pulse is 10ns, and the laser spot radius is 0.5mm. The material parameters of 316L steel are shown in Table 1.

TABLE 1. Material parameters of 316L steel.

Parameters	Value
Young modulus (GPa)	195
Heat conduction (W/m·k)	80.4
Poisson ratio	0.3
Density(kg/m3)	7980
Thermal diffusion coefficient (10^{-5}/K)	19.0×10-6
Specific heat(J/kg·k)	502

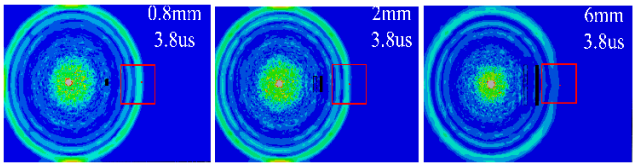

FIGURE 3. Simulation waveform of laser ultrasound.

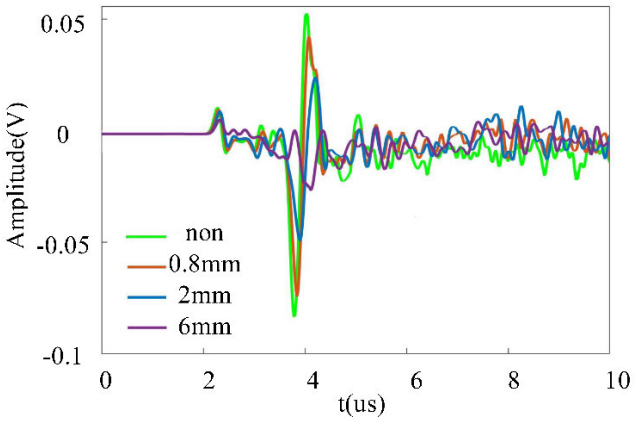

FIGURE 4. Time domain diagrams of surface waves received in different defects.

C. ANALYSIS OF SIMULATION RESULTS

The 3D finite element simulation nephogram is shown in Fig. 3. When there is a surface defect, the surface wave will interact with the defect to produce reflected wave and transmitted wave. Among them, the reflected wave interferes with the incident wave and changes weakly, which is not conducive to the analysis. As shown in the red box, with the increase of defect length, the transmission wave energy band becomes weaker and reaches the receiving point later. Therefore, in this article, the size of defects is analyzed by the change of transmitted wave. Figure 4 represents A-scan time domain diagram of non defect and different defect lengths in the same excitation and receiving positions. The larger the defect is, the more obvious the amplitude attenuation of the transmitted signal is and the longer the arrival time is. It shows that the amplitude and time characteristics of transmission wave can be used for defect length detection.

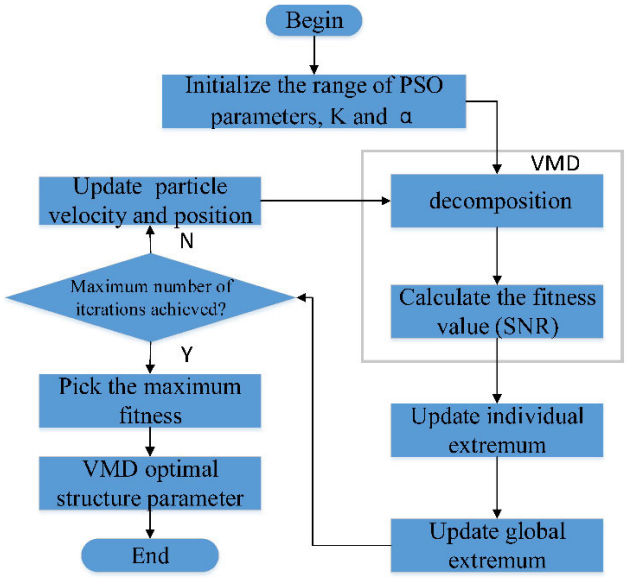

FIGURE 5. VMD parameter optimization process based on PSO.

III. VMD PARAMETER OPTIMIZATION BASED PSO

VMD is a non recursive signal decomposition method, which can adaptively decompose ultrasonic signals into a series of modes. Each mode is filtered based on the center frequency and limited bandwidth. In order to effectively remove the interference and extract the information of different defects, VMD is used to decompose the original signal to obtain several eigenfunctions, namely IMF component [36]. The optimal IMF component is selected as the damage signal. However, the premise and key of VMD to decompose signals accurately are the number of modal components K and the quadratic penalty factor α. In this article, PSO intelligent optimization algorithm is used to optimize this parameter, the particle update strategy and inertia weight are improved to automatically screen out the optimal parameter combination, as shown in Fig. 5. In the process of particle updating, an adaptive function is defined as the maximum signal-to-noise ratio (SNR) between the first IMF component and the original signal. The SNR is defined as follows:

$$SNR = log_{10}(\frac{A_{signal}}{A_{noise}}). \tag{7}$$

Among them, A_{signal} is defined as the maximum amplitude of surface direct wave signal, A_{noise} is defined as the average value of local noise amplitude.

IV. EXPERIMENT AND RESULT ANALYSIS

A. SLM TECHNOLOGY AND SAMPLE

SLM is a new surface modification technology, which means coating materials with special properties on the surface of the substrate. By irradiation of high-energy density laser beam, the material and the substrate surface are rapidly melted and solidified to form a metallurgical combination. Thus, a composite cladding layer with special properties such as corrosion resistance, fatigue resistance, high hardness,

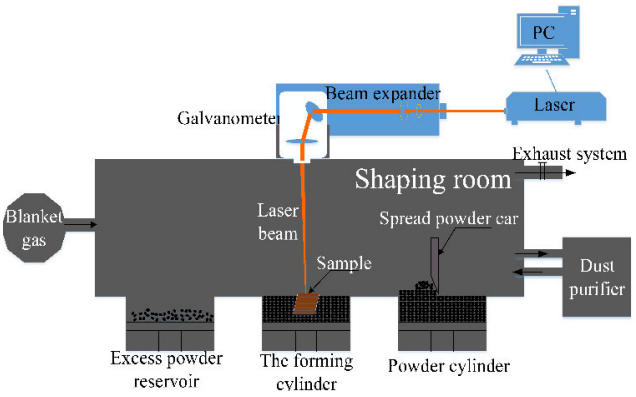

FIGURE 6. SLM technical principle diagram.

TABLE 2. SLM processing parameters.

Parameters	Value
Scanning speed (mm/s)	950
Laser energy (W)	275
Spacing (um)	80
Energy layer thickness (um)	40
Powder particle diameter (um)	10-40

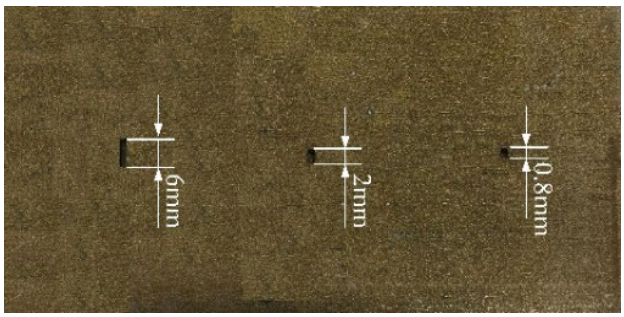

FIGURE 7. 316L steel part and artificial defects.

high wear resistance and high temperature resistance is obtained. The metal 3D printing technology based on SLM can almost replace most traditional forming methods to manufacture metal parts with complex structure, as shown in Fig. 6. SLM equipment model is BLT-s310 (Xi'an platinum Laser Forming Technology Co., Ltd.). 316L stainless steel powder is made by atomization, and the particles are almost spherical. The processing parameters are shown in Table 2. In this article, SLM technology is used to process 316L stainless steel additive parts. The length, width and height are 100mm×50mm ×5mm respectively. Three groove defects are machined on its surface. The length, width and depth are 2mm × 0.5mm × 1 mm, 0.8mm × 0.5mm × 1 mm and 6mm × 0.5mm × 1 mm respectively, as shown in Fig. 7.

B. EXPERIMENT SYSTEM

A fully non-contact laser ultrasonic B-scan system is built in this article, as shown in Fig. 8. The 316L steel test block is fixed on a two-dimensional scanning frame, and the scanning frame is controlled by computer to move along the y-axis with a step interval of 0.1 mm. The scanning mode is shown in Fig. 9. The laser and interferometer focus the spot through the focusing lens and are fixed on the optical platform. The total

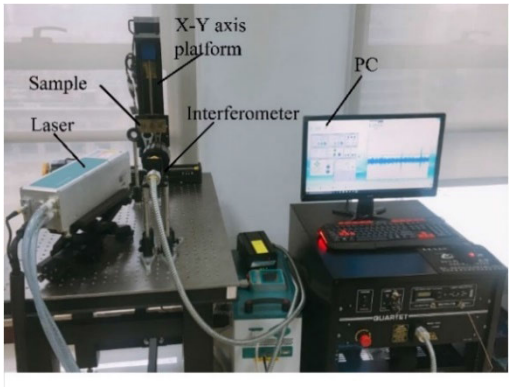

FIGURE 8. Laser ultrasonic experiment system.

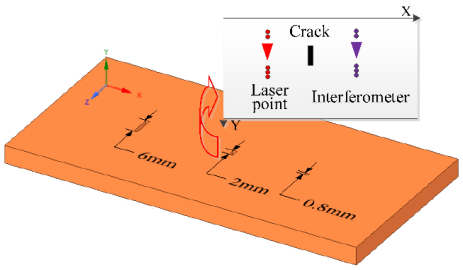

FIGURE 9. Schematic diagram of laser ultrasound scanning.

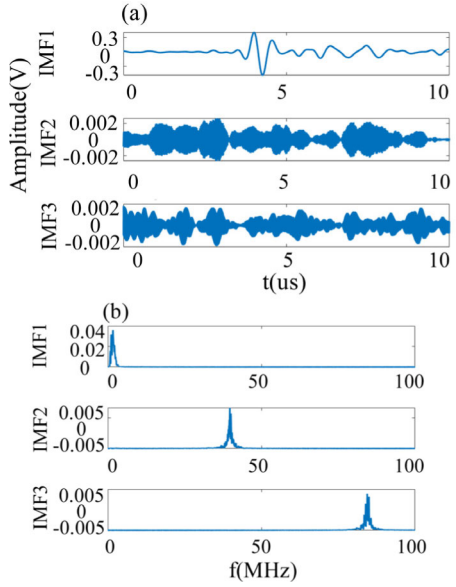

FIGURE 10. VMD decomposition results of laser ultrasonic surface wave signal (a) time domain (b) frequency domain.

scanning displacement is 20 mm, the distance between the excitation point and the receiving point is 10 mm, and the repetition rate of the laser is 20 Hz. The signal is accepted with NI acquisition card and the sampling frequency is 125 MHz.

C. EXPERIMENTAL RESULTS AND DISCUSSION

Through particle swarm optimization, the number of VMD modal components K = 3 and the second penalty factor α = 100000 are the best. On this basis, VMD is used to decompose the signal. Fig. 10 (a) (b) shows the time-domain

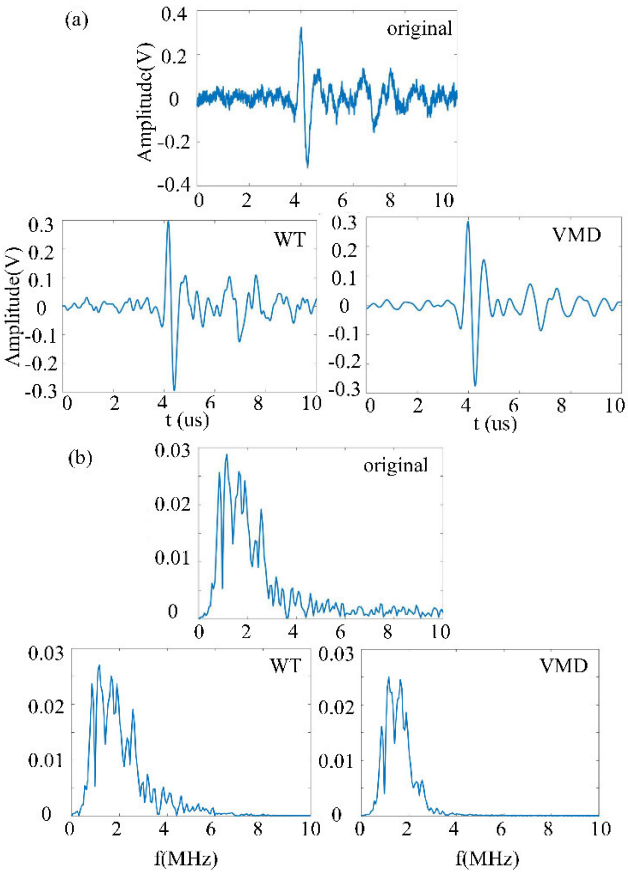

FIGURE 11. (a)Time domain and (b) frequency domain graphs of signals after different algorithms.

TABLE 3. SNR of different signals.

Signal	Original	WT	IMF1	IMF2	IMF3
SNR (dB)	3.1345	4.6683	5.1603	3.3797	3.2940

and frequency-domain decomposition results of any group of ultrasonic signals. IMF1 is the most consistent with the original signal in time domain. The frequency of IMF1 is concentrated in 0-4MHz, which is close to the actual ultrasonic signal. The IMF2 and IMF3 frequency bands are 40MHz and 80MHz respectively. The time domain display is also disordered, which is ultrasonic signal with high frequency noise. In order to compare the denoising effect of VMD, the commonly used WT algorithm is used to denoise the signal. The comparison of time domain and frequency domain of each algorithm is shown in Fig. 11. The original signal has many burr and obvious noise. After WT denoising, the signal is much more stable, but there is still obvious noise signal. The IMF1 signal has almost no burr, and the ultrasonic signal is the most obvious. The SNR of each method is shown in Table 3, in which IMF1 has the highest signal-to-noise ratio of 5.1603. Therefore, IMF1 is selected as the denoised signal of VMD.

Signals corresponding to three different locations of the 2mm defect are selected for further analysis of transmitted

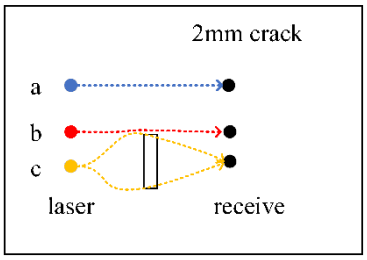

FIGURE 12. Schematic diagram of different excitation points and receiving points.

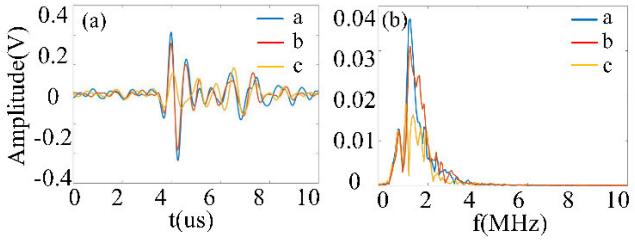

FIGURE 13. Ultrasonic signals collected at different locations from the surface defect (a) Time domain signals (b) frequency domain signals.

wave changes. a is the position away from the top of the defect, b is the same horizontal position with the top of the defect, and c is the same horizontal position with the center of the defect, as shown in Fig. 12.

As shown in Fig. 13 (a) (b), the time-domain and frequency-domain signals corresponding to the three positions are shown. It can be seen that the surface wave is not hindered by defects when it is excited at position a. The received surface wave signal is a direct wave signal, and the amplitude of the signal in time domain and frequency domain is the largest. At position b, the surface wave begins to scatter. Although most of the signals can be transmitted to the receiving point, the signal amplitude still shows attenuation, but the time delay is not obvious. At position c, due to the obvious obstruction of time and amplitude attenuation of surface wave signal are the most obvious. According to the time-frequency diagram (Fig.13 b), the frequency band of the signal is concentrated between 0 and 4MHz. The center frequency is about 1.8 MHz and the surface wave length is about 1.7 mm. With the increase of defects, the amplitude attenuation of time-frequency signal is more obvious, and the central frequency band tends to widen. Therefore, according to the surface wave transmission signals received at different positions, we can judge whether there are defects and the beginning and end of defects.

Fig. 14 (a) (b) shows the time domain and frequency domain signals corresponding to the same excitation and receiving point with different length defects. In accordance with the theory, When the defect length is smaller than the wavelength, the attenuation of transmitted wave signal is small, and the time-domain signal of A scan is close to that of intact part, so it is difficult to resolve directly. On the contrary, when the defect length is greater than or equal to

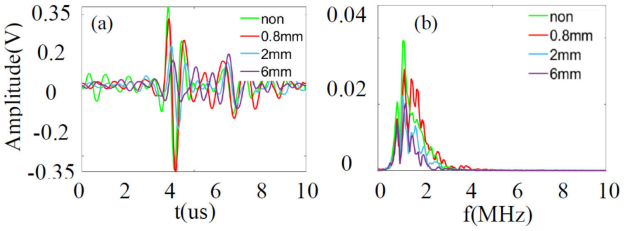

FIGURE 14. (a) Time domain (b) frequency domain signals corresponding to excitation points at the same position of different defects.

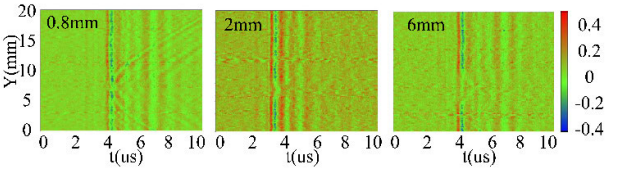

FIGURE 15. The B-scan imaging results of the original data.

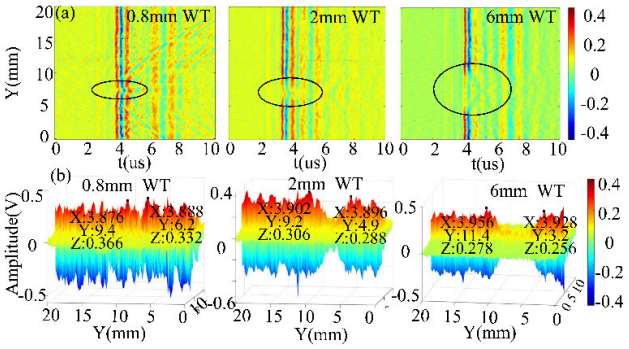

FIGURE 16. After WT denoising (a) B scanning imaging (b) three-dimensional imaging.

the wavelength, the transmitted signal changes obviously. The larger the defect, the weaker the transmitted wave amplitude signal and the more obvious the delay. Therefore, the relationship of defect length can be quantitatively analyzed according to the attenuation degree and time delay of transmission wave signal. The law of the above experimental signals is consistent with the simulation results, which shows that the surface wave detection of surface defects is highly sensitive.

According to the change of the transmitted wave signal, B-scan imaging is carried out for different length defects. There are many noise in the original signal, the effect of B-scan imaging is poor and the length of defect cannot be clearly quantified, as shown in Fig. 15. In Fig. 16 (a) and Fig. 17 (a), the imaging results after WT and VMD denoising are respectively shown. It can be seen that the imaging results of the two denoising algorithms are clearer than the original image, and the shadow area caused by defects can be clearly seen. However, the imaging results after VMD noise reduction, the energy ribbon is smooth and the defect contour is clearer than WT. Three kinds of defects with different sizes also reflect the scattering law of ultrasonic wave again, that is, the strength of transmitted wave signal depends on the length

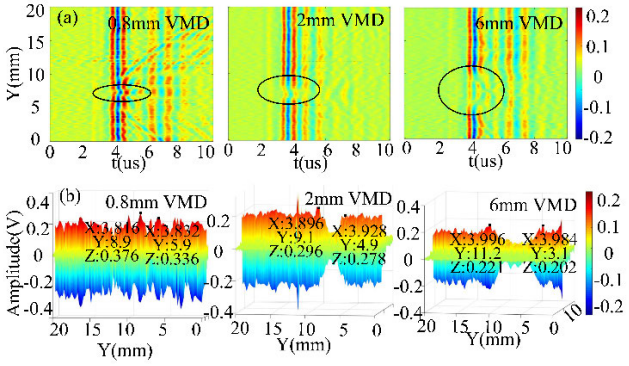

FIGURE 17. After VMD denoising (a) B scanning imaging (b) three-dimensional imaging.

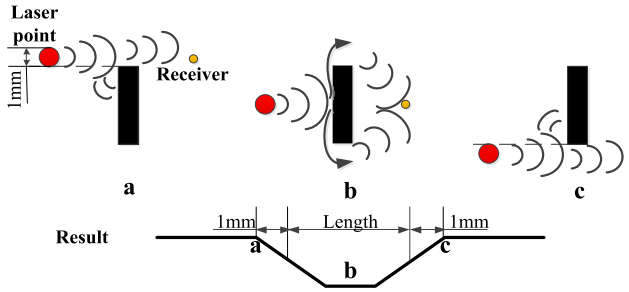

FIGURE 18. Quantitative evaluation method of laser ultrasound B-scan.

of defect. When the defect length is 0.8mm, the transmitted wave signal energy is the largest, and the corresponding transmitted energy in the black original frame is obvious, while the defect is not obvious. When the defect length is 2mm, the transmitted ribbon is obviously weaker, but the defect contour can be more obvious. When the defect length is 6mm, the transmitted wave signal and the corresponding color band almost disappears.

It is found that the spot size can not be ignored because the spot diameter is close to the minimum defect size, as shown in Fig. 18. In Fig. 18a, when the bottom of the spot is at the same height as the top of the defect, the surface wave has already started to scatter. A small part of the surface wave will be reflected back, and a large part will be diffracted to the receiving point of the interferometer at the same horizontal position. Similar to figure 18c, when the top of the spot and the bottom of the defect are in the same horizontal line, the same situation will happen. At position b, when the spot diameter is smaller than the defect length, there will be more obvious reflection, and the longer the defect is, the more obvious the reflection is, and the weaker the transmission is. At this time, the amplitude attenuation is the most obvious and the time delay is the most obvious position of all received signals. Therefore, point a is where the amplitude of the surface wave begins to weaken, and at c it is the end point. Therefore, in the final B-scan results, the distance between the start point and the end point also includes the diameter of two light spots. As long as the distance ac is subtracted by 2mm, the defect length is obtained. Based on this, the quantitative detection of defects with different lengths is realized.

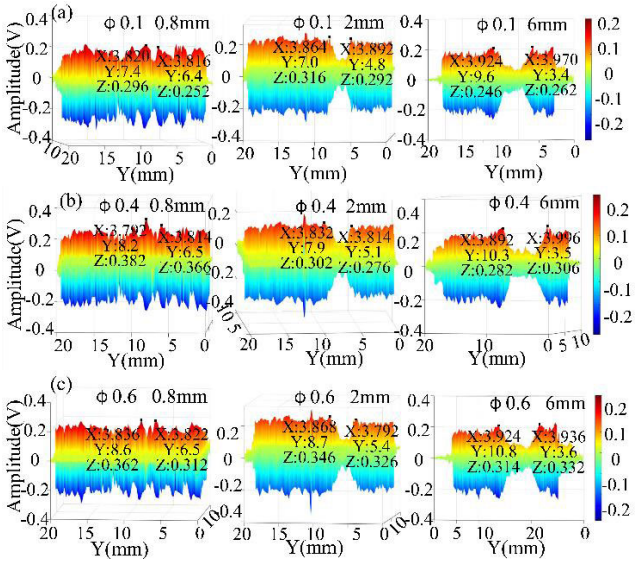

FIGURE 19. Quantitative 3D imaging maps corresponding to different excitation source diameters (a) φ0.1 (b) φ0.4 (c) φ0.6.

TABLE 4. Summary of defect quantitative results.

Situation	Quantitative results (mm)		
actual	0.8	2	6
φ1.0, WT	1.2	2.3	6.2
φ1.0, VMD	1.0	2.2	6.1
φ0.6, VMD	0.9	2.1	6.0
φ0.4, VMD	0.9	2.0	6.0
φ0.1, VMD	0.8	2.0	6.0

In order to verify this idea, we use the lens to modulate the size of different excitation spot, which are 0.1 mm, 0.4 mm and 0.6 mm, respectively. The same scanning experiment is used for the test block, and the imf1 component is obtained by VMD decomposition of the signal. The three-dimensional imaging views obtained by different spot sizes are shown in Fig. 19. The quantitative results are shown in Table 4. The results are reduced by twice the spot diameter.

The results show that the spot size does affect the accurate quantification of small defects by B-scan. The smaller the spot, the smaller the influence. As the experimental scanning interval is 0.1mm, the pixel of B-scan imaging is 0.1mm. Therefore, when the absolute error is less than 0.1mm, the image cannot be resolved. Therefore, when the excitation point diameter is 0.1mm, the relative error between the quantitative result and the actual value is 0%. When the excitation point diameter is 1mm, the precision quantitative result processed by VMD algorithm is about 10% higher than that of WPT method.

V. SUMMARY AND FUTURE WORK

In this article, a completely non-contact laser ultrasonic B-scan inspection platform is built to quantitatively detect the surface length defects of 316L stainless steel manufactured by SLM process. In order to realize the accurate quantification of defects, the VMD algorithm is used to denoise the signal, and

the denoising results are compared with WT algorithm. The imaging accuracy of VMD is improved about 10% compared with WT denoising, and the signal is more stable. In addition, the spot size has a great influence on the quantitative results: smaller spot will improve the quantitative accuracy. The experimental results show that the laser ultrasonic testing technology has high sensitivity to the surface defects of the specimen, and can effectively determine the location and length of the defects.

However, the technology has some limitations, such as laser scanning efficiency and signal optimization. In the future research, the probability of detection of natural cracks will be carried out. Other issues to be addressed in the future can be applied practically include: (a) optimizing the experimental method to improve the laser scanning efficiency; (b) optimize signal processing methods to improve signal quality.

REFERENCES

[1] Z. H. Liu, D. Q. Zhang, S. L. Sing, C. K. Chua, and L. E. Loh, "Interfacial characterization of SLM parts in multi-material processing: Metallurgical diffusion between 316L stainless steel and C18400 copper alloy," *Mater. Characterization*, vol. 94, pp. 116–125, Aug. 2014.

[2] X. Zhang, S. Y. Tang, H. Y. Zhao, S. Q. Guo, N. Li, B. B. Sun, and B. Q. Chen, "Research status and key technologies of 3D printing," *J. Mater. Eng.*, vol. 44, pp. 122–128, Feb. 2016.

[3] M. Schmidt, M. Merklein, D. Bourell, D. Dimitrov, T. Hausotte, K. Wegener, L. Overmeyer, F. Vollertsen, and G. N. Levy, "Laser based additive manufacturing in industry and academia," *CIRP Ann.*, vol. 66, no. 2, pp. 561–583, 2017, doi: 10.1016/j.cirp.2017.05.011.

[4] J. J. Lewandowski and M. Seifi, "Metal additive manufacturing: A review of mechanical properties," *Annu. Rev. Mater. Res.*, vol. 46, no. 1, pp. 151–186, Jul. 2016, doi: 10.1146/annurev-matsci-070115-032024.

[5] H. Rieder, M. Spies, J. Bamberg, and B. Henkel, "On-and offline ultrasonic characterization of components built by SLM additive manufacturing," *Rev. Prog. QNDE*, vol. 1706, Feb. 2016, Art. no. 130002, doi: 10.1063/1.4940605.

[6] W. E. Frazier, "Metal additive manufacturing: A review," *J. Mater. Eng. Perform.*, vol. 23, no. 6, pp. 1917–1928, Apr. 2014, doi: 10.1007/s11665-014-0958-z.

[7] T. DebRoy, H. L. Wei, J. S. Zuback, T. Mukherjee, J. W. Elmer, J. O. Milewski, A. M. Beese, A. Wilson-Heid, A. De, and W. Zhang, "Additive manufacturing of metallic components—Process, structure and properties," *Prog. Mater. Sci.*, vol. 92, pp. 112–224, Mar. 2018, doi: 10.1016/j.pmatsci.2017.10.001.

[8] D. Herzog, V. Seyda, E. Wycisk, and C. Emmelmann, "Additive manufacturing of metals," *Acta Mater.*, vol. 117, pp. 371–392, Sep. 2016, doi: 10.1016/j.actamat.2016.07.019.

[9] Y. Zhai, H. Galarraga, and D. A. Lados, "Microstructure, static properties, and fatigue crack growth mechanisms in Ti-6Al-4 V fabricated by additive manufacturing: LENS and EBM," *Eng. Failure Anal.*, vol. 69, pp. 3–14, Nov. 2016, doi: 10.1016/j.engfailanal.2016.05.036.

[10] N. P. Aleshin, M. V. Grigor'ev, N. A. Shchipakov, M. A. Prilutskii, and V. V. Murashov, "Applying nondestructive testing to quality control of additive manufactured parts," *Russian J. Nondestruct. Test.*, vol. 52, no. 10, pp. 600–609, Dec. 2016, doi: 10.1134/S1061830916100028.

[11] P. Nilsson, A. Appelgren, P. Henrikson, and A. Runnemalm, "Automatic ultrasonic testing for metal deposition," in *Proc. 18th World Conf. Nondestruct. Test.*, Durban, South Africa, 2012, pp. 1–10.

[12] A. du Plessis, I. Yadroitsev, I. Yadroitsava, and S. G. Le Roux, "X-ray microcomputed tomography in additive manufacturing: A review of the current technology and applications," *3D Printing Additive Manuf.*, vol. 5, no. 3, pp. 227–247, Sep. 2018, doi: 10.1089/3dp.2018.0060.

[13] V. Dikshit *et al.*, "Quasi-static indentation analysis on three-dimensional printed continuous-fiber sandwich composites," *J. Sandwich Struct. Mater.*, pp. 1–20, Mar. 2019, doi: 10.1177/1099636219836058.

[14] A. du Plessis, I. Yadroitsava, and I. Yadroitsev, "Effects of defects on mechanical properties in metal additive manufacturing: A review focusing on X-ray tomography insights," *Mater. Des.*, vol. 187, pp. 227–247, Feb. 2020, doi: 10.1016/j.matdes.2019.108385.

[15] G. Ziółkowski, E. Chlebus, P. Szymczyk, and J. Kurzac, "Application of X-ray CT method for discontinuity and porosity detection in 316L stainless steel parts produced with SLM technology," *Arch. Civil Mech. Eng.*, vol. 14, no. 4, pp. 608–614, Aug. 2014, doi: 10.1016/j.acme.2014.02.003.

[16] F. Zanini, P. Hermanek, J. Rathore, W. W. Wits, and S. Carmignato, "Investigation on the accuracy of CT porosity analysis of additive manufactured metallic parts," in *Proc. Int. Symp. Digit. Ind. Radiol. Comput. Tomogr.*, 2015, pp. 22–25.

[17] N. Kobayashi, S. Yamamoto, A. Sugawara, M. Nakane, D. Tsuji, T. Hino, T. Terada, and M. Ochiai, "Fundamental experiments of eddy current testing for additive manufacturing metallic material toward in-process inspection," *AIP Conf. Proc.*, vol. 2102, 2019, Art. no. 070003, doi: 10.1063/1.5099803.

[18] A. du Plessis, S. G. le Roux, J. Els, G. Booysen, and D. C. Blaine, "Application of microCT to the non-destructive testing of an additive manufactured titanium component," *Case Stud. Nondestruct. Test. Eval.*, vol. 4, pp. 1–7, Nov. 2015, doi: 10.1016/j.csndt.2015.09.001.

[19] Y. Gao, G. Y. Tian, K. Li, J. Ji, P. Wang, and H. Wang, "Multiple cracks detection and visualization using magnetic flux leakage and eddy current pulsed thermography," *Sens. Actuators A, Phys.*, vol. 234, pp. 269–281, Oct. 2015, doi: 10.1016/j.sna.2015.09.011.

[20] Z. Zhu, H. Sui, L. Yu, H. Zhu, J. Zhang, and J. Peng, "Effective defect features extraction for laser ultrasonic signal processing by using time–frequency analysis," *IEEE Access*, vol. 7, pp. 128706–128713, 2019, doi: 10.1109/ACCESS.2019.2939262.

[21] Z. H. U. Qian, Q. I. U. Jinhao, and C. Zhang, "Application of laser ultrasonic detection method for double-layer laminated material," *Laser Optoelectron. Prog.*, vol. 53, no. 3, 2016, Art. no. 031402, doi: 10.3788/LOP53.031402.

[22] Y.-K. An, B. Park, and H. Sohn, "Complete noncontact laser ultrasonic imaging for automated crack visualization in a plate," *Smart Mater. Struct.*, vol. 22, no. 2, Jan. 2013, Art. no. 025022.

[23] F. Lanza di Scalea and R. E. Green, "High-sensitivity laser-based ultrasonic C-scan system for materials inspection," *Experim. Mech.*, vol. 39, no. 4, pp. 329–334, Dec. 1999, doi: 10.1007/BF02329813.

[24] I. Pelivanov, T. Buma, J. Xia, C.-W. Wei, and M. O'Donnell, "A new fiber-optic non-contact compact laser-ultrasound scanner for fast non-destructive testing and evaluation of aircraft composites," *J. Appl. Phys.*, vol. 115, no. 11, Mar. 2014, Art. no. 113105, doi: 10.1063/1.4868463.

[25] N. Toyama, J. Ye, W. Kokuyama, and S. Yashiro, "Non-contact ultrasonic inspection of impact damage in composite laminates by visualization of Lamb wave propagation," *Appl. Sci.*, vol. 9, no. 1, p. 46, Dec. 2018, doi: 10.3390/app9010046.

[26] A. Furusawa, Y. Takenaka, and A. Nishimura, "Proposal of laser-induced ultrasonic guided wave for corrosion detection of reinforced concrete structures in fukushima daiichi nuclear power plant decommissioning site," *Appl. Sci.*, vol. 9, no. 17, p. 3544, Aug. 2019, doi: 10.3390/app9173544.

[27] J. Yu, D. Zhang, H. Li, C. Song, X. Zhou, S. Shen, G. Zhang, Y. Yang, and H. Wang, "Detection of internal holes in additive manufactured Ti-6Al-4 V part using laser ultrasonic testing," *Appl. Sci.*, vol. 10, no. 1, p. 365, Jan. 2020, doi: 10.3390/app10010365.

[28] D. Lévesque, C. Bescond, M. Lord, X. Cao, P. Wanjara, and J. P. Monchalin, "Inspection of additive manufactured parts using laser ultrasonics," *AIP Conf. Proc.*, vol. 1706, Feb. 2016, Art. no. 130003, doi: 10.1063/1.4940606.

[29] D. Cerniglia, M. Scafidi, A. Pantano, and J. Rudlin, "Inspection of additive-manufactured layered components," *Ultrasonics*, vol. 62, pp. 292–298, Sep. 2015, doi: 10.1016/j.ultras.2015.06.001.

[30] P. A. Fomitchov, A. K. Kromin, S. Krishnaswamy, and J. D. Achenbach, "Imaging of damage in sandwich composite structures using a scanning laser source technique," *Compos. B, Eng.*, vol. 35, nos. 6–8, pp. 557–562, Sep. 2004, doi: 10.1016/j.compositesb.2004.04.007.

[31] K. Zhang, Z. Zhou, and L. Ma, "Research on a laser ultrasound method for testing the quality of a nuclear radiation protection structure," *Meas. Sci. Technol.*, vol. 28, no. 2, Dec. 2016, Art. no. 025204.

[32] B. Liang, S. D. Iwnicki, Y. Zhao, and D. Crosbee, "Railway wheel-flat and rail surface defect modelling and analysis by time–frequency techniques," *Vehicle Syst. Dyn.*, vol. 51, no. 9, pp. 1403–1421, Sep. 2013, doi: 10.1080/00423114.2013.804192.

[33] F. Wang, Z. Xing, Y. Qin, J. Li, and Y. Chen, "The analysis of axle box vibration signal based on frequency slice wavelet transform," in *Proc. Int. Conf. Comput. Comput. Sci. (ICCCS)*, Jan. 2015, pp. 1312–1316, doi: 10.1109/ICCACS.2015.7361324.
[34] U. Satija, N. Trivedi, G. Biswal, and B. Ramkumar, "Specific emitter identification based on variational mode decomposition and spectral features in single hop and relaying scenarios," *IEEE Trans. Inf. Forensics Security*, vol. 14, no. 3, pp. 581–591, Mar. 2019, doi: 10.1109/TIFS.2018.2855665.
[35] P. Singh and G. Pradhan, "Variational mode decomposition based ECG denoising using non-local means and wavelet domain filtering," *Australas. Phys. Eng. Sci. Med.*, vol. 41, no. 4, pp. 891–904, Sep. 2018, doi: 10.1007/s13246-018-0685-0.
[36] X. Jiang, C. Shen, J. Shi, and Z. Zhu, "Initial center frequency-guided VMD for fault diagnosis of rotating machines," *J. Sound Vibrat.*, vol. 435, pp. 36–55, Nov. 2018, doi: 10.1016/j.jsv.2018.07.039.
[37] X. Yan and M. Jia, "A novel optimized SVM classification algorithm with multi-domain feature and its application to fault diagnosis of rolling bearing," *Neurocomputing*, vol. 313, pp. 47–64, Nov. 2018, doi: 10.1016/j.neucom.2018.05.002.
[38] G.-D. Sun, Y.-R. Wang, C.-F. Sun, and Q. Jin, "Intelligent detection of a planetary gearbox composite fault based on adaptive separation and deep learning," *Sensors*, vol. 19, no. 23, p. 5222, Nov. 2019, doi: 10.3390/s19235222.

YI JIANG received the B.Sc. and M.Sc. degrees in mechanical engineering from Nantong University, Nantong, China, in 2013 and 2016, respectively. She is currently pursuing the Ph.D. degree with the College of Automation Engineering, Nanjing University of Aeronautics and Astronautics, Nanjing, China. She is also a Visiting Scholar with the School of Electrical and Electronic Engineering, The University of Adelaide, Australia. Her research interests include structural health monitoring and nondestructive testing.

HAITAO WANG received the bachelor's degree from Xi'an Jiaotong University, in 1991, and the master's and Ph.D. degrees from the Chinese Academy of Sciences, in 1994 and 2002, respectively. He is currently the Vice Director of the Nanjing Engineering Center Safety and Energy Saving. From 1998 to 2000, he worked with the Max Planck Institute for Extraterrestrial Physics (MPE), Munich, as a Scientist. During 2010, he was the Director of the Department of the Fly Test, Shanghai Aircraft Design and Research Institute, and Commercial Aircraft Corporation of China (COMAC). He is also a member of the Council of Jiangsu Society for Nondestructive Testing and the Measurement of the Stress-Strain and the Structural Health Monitoring Branch of the China Instrument and Control Society.

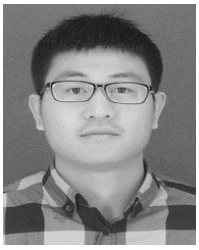

SHUAI CHEN received the M.Sc. degree from the Inner Mongolia University of Science and Technology, Inner Mongolia, China. He is currently pursuing the Ph.D. degree with the College of Automation Engineering, Nanjing University of Aeronautics and Astronautics, Nanjing, China. His research interests include nondestructive testing and mechanical failure diagnosis.

QING ZHANG received the B.Sc. degree from North China Electric Power University, in 2012, and the Ph.D. degree from the Huazhong University of Science and Technology, China, in 2018.

She is currently a Postdoctoral Researcher with the College of Automation Engineering, Nanjing University of Aeronautics and Astronautics, Nanjing, China. Her current research interests include electromagnetic nondestructive testing and evaluation, modeling of eddy current fields and computation, signal processing, and sensors.

PAN HU received the B.Sc. and M.Sc. degrees in electrical engineering and automation from Yangzhou University, Yangzhou, China, in 2012 and 2015, respectively. He is currently pursuing the Ph.D. degree with the College of Automation Engineering, Nanjing University of Aeronautics and Astronautics, Nanjing, China. He is also a Visiting Scholar with the Department of Civil and Environmental Engineering, University of Illinois at Urbana–Champaign, Urbana, IL, USA. His research interests include structural health monitoring and wireless sensor networks.

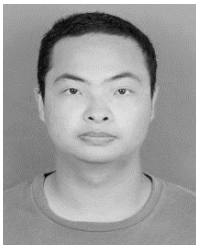

XIN LI received the master's degree from Nanchang Hangkong University, in 2018. He is currently pursuing the Ph.D. degree with the Nanjing University of Aeronautics and Astronautics. His research interests include ultrasound detection technology and ultrasound imaging algorithm and so on.

KAI ZHENG received the B.Sc. degree from the Nanjing University of Chemical Technology, in 1989, and the M.Sc. and Ph.D. degrees from Nanjing University, Nanjing, China, in 2004 and 2006, respectively. His research interests include structural health monitoring and nondestructive testing. He is currently the Core Member of the IEEE Far East Forum on Nondestructive Evaluation.

HAILONG WANG received the B.Sc. and M.Sc. degrees in mechatronic engineering from Northwestern Polytechnical University, Xi'an, China. His research interests include structural health monitoring and nondestructive testing. He was a recipient of the Second Prize of Provincial Science and Technology Progress Award.